UNIVERSITY OF AMSTERDAM

UvA-DARE (Digital Academic Repository)

XRISM Reveals Low Nonthermal Pressure in the Core of the Hot, Relaxed Galaxy Cluster A2029

XRISM Collaboration; Audard, Marc; Costantini, Elisa; Vink, Jacco

DOI
10.3847/2041-8213/ada7cd

Publication date
2025

Document Version
Final published version

Published in
Astrophysical Journal Letters

License
CC BY

Link to publication

Citation for published version (APA):
XRISM Collaboration, Audard, M., Costantini, E., & Vink, J. (2025). XRISM Reveals Low Nonthermal Pressure in the Core of the Hot, Relaxed Galaxy Cluster A2029. *Astrophysical Journal Letters*, *982*(1), Article L5. https://doi.org/10.3847/2041-8213/ada7cd

General rights
It is not permitted to download or to forward/distribute the text or part of it without the consent of the author(s) and/or copyright holder(s), other than for strictly personal, individual use, unless the work is under an open content license (like Creative Commons).

Disclaimer/Complaints regulations
If you believe that digital publication of certain material infringes any of your rights or (privacy) interests, please let the Library know, stating your reasons. In case of a legitimate complaint, the Library will make the material inaccessible and/or remove it from the website. Please Ask the Library: https://uba.uva.nl/en/contact, or a letter to: Library of the University of Amsterdam, Secretariat, P.O. Box 19185, 1000 GD Amsterdam, The Netherlands. You will be contacted as soon as possible.

UvA-DARE is a service provided by the library of the University of Amsterdam (https://dare.uva.nl)

Download date:05 Sept 2026

The Astrophysical Journal Letters, 982:L5 (9pp), 2025 March 20 https://doi.org/10.3847/2041-8213/ada7cd
© 2025. The Author(s). Published by the American Astronomical Society.
OPEN ACCESS

XRISM Reveals Low Nonthermal Pressure in the Core of the Hot, Relaxed Galaxy Cluster A2029

XRISM Collaboration, Marc Audard[1], Hisamitsu Awaki[2], Ralf Ballhausen[3,4,5], Aya Bamba[6], Ehud Behar[7], Rozenn Boissay-Malaquin[4,5,8], Laura Brenneman[9], Gregory V. Brown[10], Lia Corrales[11], Elisa Costantini[12], Renata Cumbee[4], Maria Diaz Trigo[13], Chris Done[14], Tadayasu Dotani[15], Ken Ebisawa[15], Megan E. Eckart[10], Dominique Eckert[1], Satoshi Eguchi[16], Teruaki Enoto[17], Yuichiro Ezoe[18], Adam Foster[9], Ryuichi Fujimoto[15], Yutaka Fujita[18], Yasushi Fukazawa[19], Kotaro Fukushima[15], Akihiro Furuzawa[20], Luigi Gallo[21], Javier A. García[4,22], Liyi Gu[12], Matteo Guainazzi[23], Kouichi Hagino[6], Kenji Hamaguchi[4,5,8], Isamu Hatsukade[24], Katsuhiro Hayashi[15], Takayuki Hayashi[4,5,8], Natalie Hell[10], Edmund Hodges-Kluck[4], Ann Hornschemeier[4], Yuto Ichinohe[25], Manabu Ishida[15], Kumi Ishikawa[18], Yoshitaka Ishisaki[18], Jelle Kaastra[12,26], Timothy Kallman[4], Erin Kara[27], Satoru Katsuda[28], Yoshiaki Kanemaru[15], Richard Kelley[4], Caroline Kilbourne[4], Shunji Kitamoto[29], Shogo Kobayashi[30], Takayoshi Kohmura[31], Aya Kubota[32], Maurice Leutenegger[4], Michael Loewenstein[3,4,5], Yoshitomo Maeda[15], Maxim Markevitch[4], Hironori Matsumoto[33], Kyoko Matsushita[30], Dan McCammon[34], Brian McNamara[35], François Mernier[3,4,5], Eric D. Miller[27], Jon M. Miller[11], Ikuyuki Mitsuishi[36], Misaki Mizumoto[37], Tsunefumi Mizuno[38], Koji Mori[24], Koji Mukai[4,5,8], Hiroshi Murakami[39], Richard Mushotzky[3], Hiroshi Nakajima[40], Kazuhiro Nakazawa[36], Jan-Uwe Ness[41], Kumiko Nobukawa[42], Masayoshi Nobukawa[43], Hirofumi Noda[44], Hirokazu Odaka[33], Shoji Ogawa[15], Anna Ogorzalek[3,4,5], Takashi Okajima[4], Naomi Ota[45], Stephane Paltani[1], Robert Petre[4], Paul Plucinsky[9], Frederick S. Porter[4], Katja Pottschmidt[4,5,8], Kosuke Sato[28], Toshiki Sato[46], Makoto Sawada[29], Hiromi Seta[18], Megumi Shidatsu[2], Aurora Simionescu[12], Randall Smith[9], Hiromasa Suzuki[15], Andrew Szymkowiak[47], Hiromitsu Takahashi[19], Mai Takeo[28], Toru Tamagawa[25], Keisuke Tamura[4,5,8], Takaaki Tanaka[48], Atsushi Tanimoto[49], Makoto Tashiro[15,28], Yukikatsu Terada[15,28], Yuichi Terashima[2], Yohko Tsuboi[50], Masahiro Tsujimoto[15], Hiroshi Tsunemi[33], Takeshi Tsuru[17], Hiroyuki Uchida[17], Nagomi Uchida[15], Yuusuke Uchida[31], Hideki Uchiyama[51], Yoshihiro Ueda[52], Shinichiro Uno[53], Jacco Vink[12,54], Shin Watanabe[15], Brian J. Williams[4], Satoshi Yamada[55], Shinya Yamada[29], Hiroya Yamaguchi[15], Kazutaka Yamaoka[36], Noriko Yamasaki[15], Makoto Yamauchi[24], Shigeo Yamauchi[56], Tahir Yaqoob[4,5,8], Tomokage Yoneyama[50], Tessei Yoshida[15], Mihoko Yukita[4,57], Irina Zhuravleva[58], Tommaso Bartalesi[59,60], Stefano Ettori[60,61], Roman Kosarzycki[4,62], Lorenzo Lovisari[9,60], Tom Rose[35], Arnab Sarkar[27], Ming Sun[63], and Prathamesh Tamhane[63]

[1] Department of Astronomy, University of Geneva, Versoix CH-1290, Switzerland
[2] Department of Physics, Ehime University, Ehime 790-8577, Japan
[3] Department of Astronomy, University of Maryland, College Park, MD 20742, USA
[4] NASA / Goddard Space Flight Center, Greenbelt, MD 20771, USA
[5] Center for Research and Exploration in Space Science and Technology, NASA / GSFC (CRESST II), Greenbelt, MD 20771, USA
[6] Department of Physics, University of Tokyo, Tokyo 113-0033, Japan
[7] Department of Physics, Technion, Technion City, Haifa 3200003, Israel
[8] Center for Space Sciences and Technology, University of Maryland, Baltimore County (UMBC), Baltimore, MD 21250, USA
[9] Center for Astrophysics—Harvard-Smithsonian, Cambridge, MA 02138, USA
[10] Lawrence Livermore National Laboratory, Livermore, CA 94550, USA
[11] Department of Astronomy, University of Michigan, Ann Arbor, MI 48109, USA
[12] SRON Netherlands Institute for Space Research, Leiden, The Netherlands
[13] ESO, Karl-Schwarzschild-Strasse 2, 85748, Garching bei München, Germany
[14] Centre for Extragalactic Astronomy, Department of Physics, University of Durham, Durham DH1 3LE, UK
[15] Institute of Space and Astronautical Science (ISAS), Japan Aerospace Exploration Agency (JAXA), Kanagawa 252-5210, Japan
[16] Department of Economics, Kumamoto Gakuen University, Kumamoto 862-8680, Japan
[17] Department of Physics, Kyoto University, Kyoto 606-8502, Japan
[18] Department of Physics, Tokyo Metropolitan University, Tokyo 192-0397, Japan
[19] Department of Physics, Hiroshima University, Hiroshima 739-8526, Japan
[20] Department of Physics, Fujita Health University, Aichi 470-1192, Japan
[21] Department of Astronomy and Physics, Saint Mary's University, Nova Scotia B3H 3C3, Canada
[22] California Institute of Technology, Pasadena, CA 91125, USA
[23] European Space Agency (ESA), European Space Research and Technology Centre (ESTEC), 2200 AG Noordwijk, The Netherlands
[24] Faculty of Engineering, University of Miyazaki, 1-1 Gakuen-Kibanadai-Nishi, Miyazaki, Miyazaki 889-2192, Japan
[25] RIKEN Nishina Center, Saitama 351-0198, Japan
[26] Leiden Observatory, University of Leiden, P.O. Box 9513, NL-2300 RA, Leiden, The Netherlands
[27] Kavli Institute for Astrophysics and Space Research, Massachusetts Institute of Technology, MA 02139, USA; milleric@mit.edu
[28] Department of Physics, Saitama University, Saitama 338-8570, Japan
[29] Department of Physics, Rikkyo University, Tokyo 171-8501, Japan
[30] Faculty of Physics, Tokyo University of Science, Tokyo 162-8601, Japan
[31] Faculty of Science and Technology, Tokyo University of Science, Chiba 278-8510, Japan
[32] Department of Electronic Information Systems, Shibaura Institute of Technology, Saitama 337-8570, Japan
[33] Department of Earth and Space Science, Osaka University, Osaka 560-0043, Japan
[34] Department of Physics, University of Wisconsin, WI 53706, USA
[35] Department of Physics & Astronomy, Waterloo Centre for Astrophysics, University of Waterloo, Ontario N2L 3G1, Canada

[36] Department of Physics, Nagoya University, Aichi 464-8602, Japan
[37] Science Research Education Unit, University of Teacher Education Fukuoka, Fukuoka 811-4192, Japan
[38] Hiroshima Astrophysical Science Center, Hiroshima University, Hiroshima 739-8526, Japan
[39] Department of Data Science, Tohoku Gakuin University, Miyagi 984-8588, Japan
[40] College of Science and Engineering, Kanto Gakuin University, Kanagawa 236-8501, Japan
[41] European Space Agency (ESA), European Space Astronomy Centre (ESAC), E-28692 Madrid, Spain
[42] Department of Science, Faculty of Science and Engineering, KINDAI University, Osaka 577-8502, Japan
[43] Department of Teacher Training and School Education, Nara University of Education, Nara 630-8528, Japan
[44] Astronomical Institute, Tohoku University, Miyagi 980-8578, Japan
[45] Department of Physics, Nara Women's University, Nara 630-8506, Japan
[46] School of Science and Technology, Meiji University, Kanagawa, 214-8571, Japan
[47] Yale Center for Astronomy and Astrophysics, Yale University, CT 06520-8121, USA
[48] Department of Physics, Konan University, Hyogo 658-8501, Japan
[49] Graduate School of Science and Engineering, Kagoshima University, Kagoshima, 890-8580, Japan
[50] Department of Physics, Chuo University, Tokyo 112-8551, Japan
[51] Faculty of Education, Shizuoka University, Shizuoka 422-8529, Japan
[52] Department of Astronomy, Kyoto University, Kyoto 606-8502, Japan
[53] Nihon Fukushi University, Shizuoka 422-8529, Japan
[54] Anton Pannekoek Institute, the University of Amsterdam, Postbus 942491090 GE Amsterdam, The Netherlands
[55] RIKEN Cluster for Pioneering Research, Saitama 351-0198, Japan
[56] Department of Physics, Faculty of Science, Nara Women's University, Nara 630-8506, Japan
[57] Johns Hopkins University, MD 21218, USA
[58] Department of Astronomy and Astrophysics, University of Chicago, Chicago, IL 60637, USA
[59] Dipartimento di Fisica e Astronomia "Augusto Righi"—Alma Mater Studiorum—Università di Bologna, I-40129 Bologna, Italy
[60] INAF, Osservatorio di Astrofisica e Scienza dello Spazio, 40129 Bologna, Italy
[61] INFN, Sezione di Bologna, 40127 Bologna, Italy
[62] Department of Physics, The George Washington University, Washington, DC 20052, USA
[63] Department of Physics and Astronomy, The University of Alabama in Huntsville, Huntsville, AL 35899, USA
Received 2024 November 26; revised 2025 January 7; accepted 2025 January 8; published 2025 March 12

Abstract

We present XRISM Resolve observations of the core of the hot, relaxed galaxy cluster Abell 2029 (A2029). We find that the line-of-sight bulk velocity of the intracluster medium (ICM) within the central 180 kpc is at rest with respect to the brightest cluster galaxy, with a 3σ upper limit of $|v_{\rm bulk}| < 100\,{\rm km\,s^{-1}}$. We robustly measure the field-integrated ICM velocity dispersion to be $\sigma_v = 169 \pm 10\,{\rm km\,s^{-1}}$, obtaining similar results for both single-temperature and two-temperature plasma models to account for the cluster cool core. This result, if ascribed to isotropic turbulence, implies a subsonic ICM with Mach number $\mathcal{M}_{\rm 3D} \approx 0.22$ and a nonthermal pressure fraction of $2.6 \pm 0.3\%$. The turbulent velocity is similar to what was measured in the core of the Perseus cluster by Hitomi, but here in a more massive cluster with an ICM temperature of 7 keV, the limit on the nonthermal pressure fraction is even more stringent. Our result is consistent with expectations from simulations of relaxed clusters, but it is on the low end of the predicted distribution, indicating that A2029 is an exceptionally relaxed cluster with no significant impacts from either a recent minor merger or active galactic nucleus activity.

Unified Astronomy Thesaurus concepts: Galaxy clusters (584); Intracluster medium (858); High resolution spectroscopy (2096)

1. Introduction

In the hierarchical structure formation paradigm, galaxy clusters are thought to grow over cosmic time through successive mergers and accretion of material from the cosmic web (e.g., N. Werner et al. 2008; D. Eckert et al. 2015; T. H. Reiprich et al. 2021; A. Sarkar et al. 2022). The kinetic energy injected by successive merging events is released into the hot intracluster medium (ICM) and virialized, eventually turning into heat (A. V. Kravtsov & S. Borgani 2012). However, the sound crossing time in the medium can be as large as 1 Gyr, such that the thermalization process is expected to be slow. At the present day, a substantial fraction of the injected energy should remain in the form of kinetic motions, either in large-scale bulk motions or in an isotropic turbulent cascade (e.g., E. T. Lau et al. 2009; F. Vazza et al. 2009; K. Nelson et al. 2014; V. Biffi et al. 2016). The remaining bulk and turbulent motions should generate shifts and broadening of the prominent X-ray plasma emission lines, which can then be used to assess the fraction of nonthermal (NT) energy within the ICM, estimate the thermalization timescale of the merging media, and constrain important plasma parameters such as its viscosity and thermal conduction.

Direct observational constraints on the NT pressure fraction in galaxy clusters are scarce. In general, the spectral resolution of the CCD detectors on observatories like Chandra, XMM-Newton, and Suzaku is insufficient to measure Doppler shifts and broadening of the X-ray emission lines (for a review, see A. Simionescu et al. 2019). Suzaku provided a few hints of large ICM bulk motions in a handful of clusters (T. Tamura et al. 2011; N. Ota & H. Yoshida 2016). More recently, a novel technique using instrumental fluorescence lines to correct the XMM-Newton EPIC pn energy scale has enabled more precise measurements of bulk motions in a number of clusters, allowing the first comparison of ICM kinematics in relaxed and merging clusters (J. S. Sanders et al. 2020; E. Gatuzz et al. 2022a, 2022b, 2023). The Hitomi X-ray observatory provided the first direct measurement

Original content from this work may be used under the terms of the Creative Commons Attribution 4.0 licence. Any further distribution of this work must maintain attribution to the author(s) and the title of the work, journal citation and DOI.

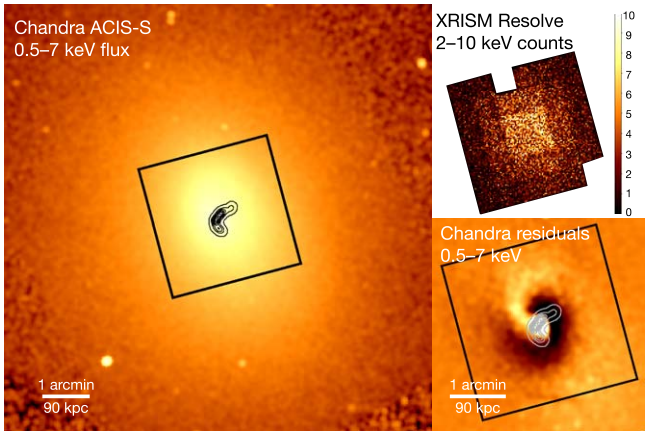

Figure 1. (Left) Chandra image of A2029 overlaid with the 1.4 GHz Very Large Array radio contours and the Resolve field of view. (Top right) Resolve counts image from the two observations combined. Locations of individual photons are randomized within each pixel in the pipeline processing. (Bottom right) Residuals after subtracting a 2D model from the Chandra image, clearly showing the sloshing spiral that extends throughout most of the Resolve field. The Chandra data used were taken in 2004.

of the line-of-sight velocity broadening in the heart of the Perseus cluster (Hitomi Collaboration et al. 2016). This result suggests that in regions strongly affected by active galactic nucleus (AGN) feedback, the velocities in the core are subsonic and provide turbulent pressure support ∼4% of the total pressure. This result on a single cluster has waited eight years for confirmation in other clusters.

Abell 2029 (A2029) is an ideal target to follow up the initial Hitomi result. It is a massive, hot galaxy cluster at $z = 0.0787$ (J. Sohn et al. 2019) that exhibits a regular X-ray morphology, as evidenced by the surface brightness concentration and by the stability of the X-ray centroid in increasingly small apertures (D. Eckert et al. 2022). This firmly classifies the cluster as dynamically relaxed (R. Cassano et al. 2010; F. Andrade-Santos et al. 2017; M. Rossetti et al. 2017). X-ray imaging spectroscopy of the cluster by Chandra (see Figure 1) indicates a mean atmospheric temperature of 7.5 ± 0.1 keV within the inner several hundred kiloparsec and a cooler, 3 keV central region with a cooling flow of several hundred solar masses per year (A. D. Lewis et al. 2002; R. Paterno-Mahler et al. 2013; C. G. Martz et al. 2020). Despite this cooling flow, its central galaxy IC 1101 exhibits none of the classical signatures of cooling, such as optical nebular emission or the blue continuum emission from massive young stars. B. T. Dullo et al. (2017) suggested a SMBH mass of $(4\text{–}10) \times 10^{10} M_{\odot}$ for IC 1101 based on its large depleted core in stellar light. With this massive SMBH, D. Prasad et al. (2024) showed that Bondi accretion of the hot gas can help to self-regulate the cool core with little precipitation.

The central galaxy hosts PKS 1508+059, a powerful, double-lobed and wide-angle radio source. In cooling cores, the jets and lobes that periodically emanate from powerful radio sources are often seen to inflate buoyant cavities in the hot, X-ray emitting atmospheres. However, the X-ray atmosphere of A2029 contains no detectable radio bubbles (T. E. Clarke et al. 2004; R. Paterno-Mahler et al. 2013; C. G. Martz et al. 2020). Unsharp masked Chandra X-ray images, constructed by subtracting a mean 2D surface brightness profile, have revealed a spiral structure extending from the central galaxy and curving out 70 kpc to the southwest, 150 kpc to the north, and 100 kpc to the east (see Figure 1). This swirling structure indicates the galaxy and its atmosphere are "sloshing" with respect to each other. These harmonic motions are normally thought to be induced by mergers, or weaker gravitational interactions with a passing halo (M. Markevitch & A. Vikhlinin 2007; J. A. ZuHone et al. 2010, 2018; A. Sarkar et al. 2023). The sloshing motion in A2029 could indicate significant relative motion between the central galaxy and atmosphere with an amplitude of several hundred kilometers per second (R. Paterno-Mahler et al. 2013).

We present XRISM (M. Tashiro et al. 2020) Resolve (Y. Ishisaki et al. 2022) observations of the inner $3 \times 3'$ (270×270 kpc) of A2029 that aim to directly measure the velocity dispersion and line-of-sight bulk velocity of the hot, bright ICM core. These relatively shallow observations are part of a larger campaign by the XRISM science team to map the velocity structure out to R_{2500} ($7.'5 \sim 670$ kpc); the much deeper outer pointings are undergoing analysis and will be presented in future work.

Throughout this Letter, we assume a ΛCDM cosmology with $H_0 = 70\ \mathrm{km\ s^{-1}\ Mpc^{-1}}$, $\Omega_m = 0.3$, and $\Omega_\Lambda = 0.7$. At the redshift of A2029 ($z = 0.0787$), $1' = 89$ kpc. All reported redshifts and velocities have been corrected to the solar system barycenter. We use the protosolar abundance table from K. Lodders & H. Palme (2009). Unless otherwise specified, reported uncertainties are 1σ.

2. Observations and Data Reduction

2.1. X-Ray Data with XRISM Resolve

The center of A2029 was observed with XRISM over two coaligned observations on 2024 January 10 and 13 (ObsIDS 000149000 and 000151000). The Resolve data for both observations were reprocessed with the XRISM team's Build 8 ftools software, applying calibration from CalDB v8 and default screening as described in the XRISM team's analysis of N132D (XRISM Collaboration 2024). The screening resulted in cleaned exposure times of 12.4 and 25.1 ks for the two observations, for a total of 37.5 ks.

The drift of the Resolve gain over an observation is tracked with occasional illumination of the focal plane with an ^{55}Fe source mounted on the filter wheel, typically during Earth occultation. The first observation received five such fiducials, with an adiabatic demagnetization refrigerator recycle in the middle of the observation, and the second observation received six. The flat-field-averaged energy scale uncertainty after gain reconstruction is $\leqslant 0.2$ eV in the 5.4–8 keV energy band (M. E. Eckart et al. 2024; F. S. Porter et al. 2024). We checked this using the calibration pixel, which is outside of the exposed array and constantly illuminated with a collimated ^{55}Fe radioactive source. We reconstructed the gain for this pixel in the standard way, using the ^{55}Fe filter wheel fiducials, and then fit the Mn Kα 5.9 keV calibration line during only the on-source times, essentially mimicking the observation of a celestial source with this pixel. This produced an energy shift of -0.12 ± 0.03 eV, consistent with the uncertainty quoted above in this energy band and comparable to other Resolve observations (e.g., XRISM Collaboration 2024).

We extracted spectra from the full array for each observation, excluding pixel 27, which in several observations has shown unexpected gain jumps that are not captured by the

^{55}Fe fiducial cadence. Only high-resolution primary ("Hp" or ITYPE = 0) events were included, as they account for more than 99% of the 2–10 keV events in each observation. This fraction ignores low-resolution secondaries ("Ls" or ITYPE = 4), which arise almost exclusively from instrumental effects at these low count rates. An image of the screened events is shown in Figure 1. The spectra were binned using the optimal binning method of J. S. Kaastra & J. A. M. Bleeker (2016), requiring at least one count per bin. A non-X-ray background (NXB) spectrum was extracted from a database of Resolve night-Earth data using rslnxbgen and weighting by the distribution of geomagnetic cutoff rigidity sampled during each observation.

Responses were generated using the Build 8 ftools, the final prelaunch suite of XRISM software provided to the science team. The redistribution matrix file (RMF) was produced with an updated CalDB file for this build, rmfparam_20190101v006, which as of this writing is the latest public CalDB file. We separated the electron loss continuum component as a more coarsely binned response file. The RMF was normalized by the Hp fraction in the 2–10 keV band, again ignoring Ls events, to account for the screened medium- and low-resolution events and ensure proper flux normalization. The ancillary response file (ARF) was constructed with xaarfgen, using an exposure-corrected 2–8 keV full-resolution Chandra image as the source model input. We also tested the analysis with a simpler point-source-model ARF, and while this alters the best-fit model normalization and derived flux, it has no effect on the reported velocity measurements within their statistical error. While we do not account explicitly for spatial–spectral mixing due to the instrumental point-spread function (PSF), we estimate from ray-tracing simulations with xrtraytrace that less than 10% of the detected 2–10 keV X-ray emission originates from outside the Resolve field of view; 97% originates within 2′ (178 kpc) of the cluster center.

2.2. Stellar Velocity with MUSE

We used the Multi-Unit Spectroscopic Explorer (MUSE) data of the central galaxy IC 1101 to determine its velocity from stellar absorption lines. There were 12 540 s MUSE WFM-AO observations from 2018 April to May, with a total exposure time of 1.8 hr, under seeing conditions of 0.″7–1.″4 and airmass of 1.16–1.32. There were also six 110 s observations on the night sky. We used the MUSE pipeline (version 2.9.0) with the ESO Recipe Execution Tool (EsoRex) to reduce the raw data, which provides a standard procedure to calibrate the individual exposures and combine them into a data cube. Further sky subtraction was performed with the Zurich Atmosphere Purge software. We then extracted the spectrum within the central 5 kpc radius and examined the spectrum with pPXF. The system redshift derived from the stellar absorption lines is $z = 0.0779 \pm 0.0001$, resulting in a brightest cluster galaxy (BCG) line-of-sight velocity uncertainty of ± 30 km s^{-1}. J. Sohn et al. (2019) derived a redshift of 0.0787 for the full cluster and a redshift of 0.0778 for the BCG IC 1101, which is consistent with our result.

3. Analysis and Discussion

3.1. X-Ray Spectral Fitting and Modeling

We fit the full-field Resolve spectra using Xspec v12.14.0h (K. A. Arnaud 1996) and employing C-statistics (W. Cash 1979). For plasma model calculations, we utilized the atomic databases from AtomDB v3.0.9 (A. R. Foster et al. 2012) and SPEXACT v3.07.00 (J. S. Kaastra et al. 1996). The SPEX continuum and line emission files were converted into Xspec-readable format, enabling us to directly compare results between two databases and ensuring a consistent approach across all underlying assumptions and fitting procedures. To model ICM plasma in both databases, we adopted a velocity-broadened collisional-equilibrium model (bapec in Xspec), allowing for a single redshift and velocity broadening in addition to the plasma thermal broadening. We applied both single-temperature (1T) and two-temperature (2T) models to explore whether the cool core affected the velocity measurements. A multiplicative absorption model (TBabs in XSPEC; J. Wilms et al. 2000) was included to account for the line-of-sight Galactic neutral column, with $N_{\rm H}$ fixed at 3×10^{20} cm^{-2} (HI4PI Collaboration et al. 2016). All other fit parameters were allowed to vary, tied between the spectra from each observation, which were observed close enough in time that the heliocentric correction is essentially the same (+25.5 km s^{-1} for the first observation, +26.0 km s^{-1} for the second). For the 2T model, we tied the abundance, redshift, and velocity dispersion σ_v between the two components.

The best-fit model parameters are listed in Table 1, and the combined spectrum with best-fit 1T AtomDB model is shown in Figure 2. While we report the values obtained from a broadband 2–10 keV fit, fits within a narrow band around the He- and H-like Fe Kα line complexes (5.5–7 keV) produced

Table 1
Best-fit Parameters for the Central Region of A2029 in the 2–10 keV Energy Band

Parameter	AtomDB v3.0.9	SPEXACT v3.07.00
1T model—TBabs⋆bapec		
kT (keV)	$6.83^{+0.14}_{-0.13}$	$6.88^{+0.13}_{-0.13}$
Abundance ($Z_\odot$)	$0.60^{+0.02}_{-0.02}$	$0.62^{+0.02}_{-0.02}$
Redshift[a]	$0.07786^{+0.00005}_{-0.00003}$	$0.07786^{+0.00004}_{-0.00003}$
$v_{\rm bulk}$ (km s^{-1})[b]	-10^{+13}_{-7}	-9^{+11}_{-8}
σ_v (km s^{-1})	169^{+10}_{-10}	169^{+10}_{-10}
N (10^{12} cm^{-5})[c]	$4.46^{+0.08}_{-0.08}$	$4.42^{+0.08}_{-0.08}$
C-stat/dof	3892/3794	3894/3794
2T model—TBabs⋆(bapec+bapec)		
kT_1 (keV)	$5.02^{+0.34}_{-1.31}$	$4.22^{+0.52}_{-0.64}$
kT_2 (keV)	$10.85^{+1.36}_{-2.63}$	$9.91^{+1.58}_{-1.62}$
Abundance ($Z_\odot$)	$0.67^{+0.04}_{-0.04}$	$0.71^{+0.04}_{-0.04}$
Redshift[a]	$0.07785^{+0.00005}_{-0.00002}$	$0.07785^{+0.00004}_{-0.00003}$
$v_{\rm bulk}$ (km s^{-1})[b]	-13^{+13}_{-7}	-11^{+11}_{-7}
σ_v (km s^{-1})	165^{+11}_{-10}	165^{+10}_{-10}
N_1 (10^{12} cm^{-5})[c]	$3.38^{+0.4}_{-1.6}$	$2.22^{+0.5}_{-1.0}$
N_2 (10^{12} cm^{-5})[c]	$2.22^{+1.7}_{-0.4}$	$2.96^{+1.0}_{-0.5}$
C-stat/dof	3882/3791	3882/3791

Notes.
[a] Redshift is with respect to the solar system barycenter. Only statistical fitting errors are quoted, and we do not include instrumental systematic gain uncertainties.
[b] Line-of-sight bulk velocity relative to the BCG redshift derived in Section 2.2, calculated as $\Delta v = c\Delta z/(1+z)$. Only statistical fitting errors are quoted, and we do not include the BCG redshift uncertainty (± 30 km s^{-1}) or the instrumental systematic gain uncertainty.
[c] The model normalization corresponds to a 3′-radius circular region centered on A2029, since this was the model input to xaarfgen.

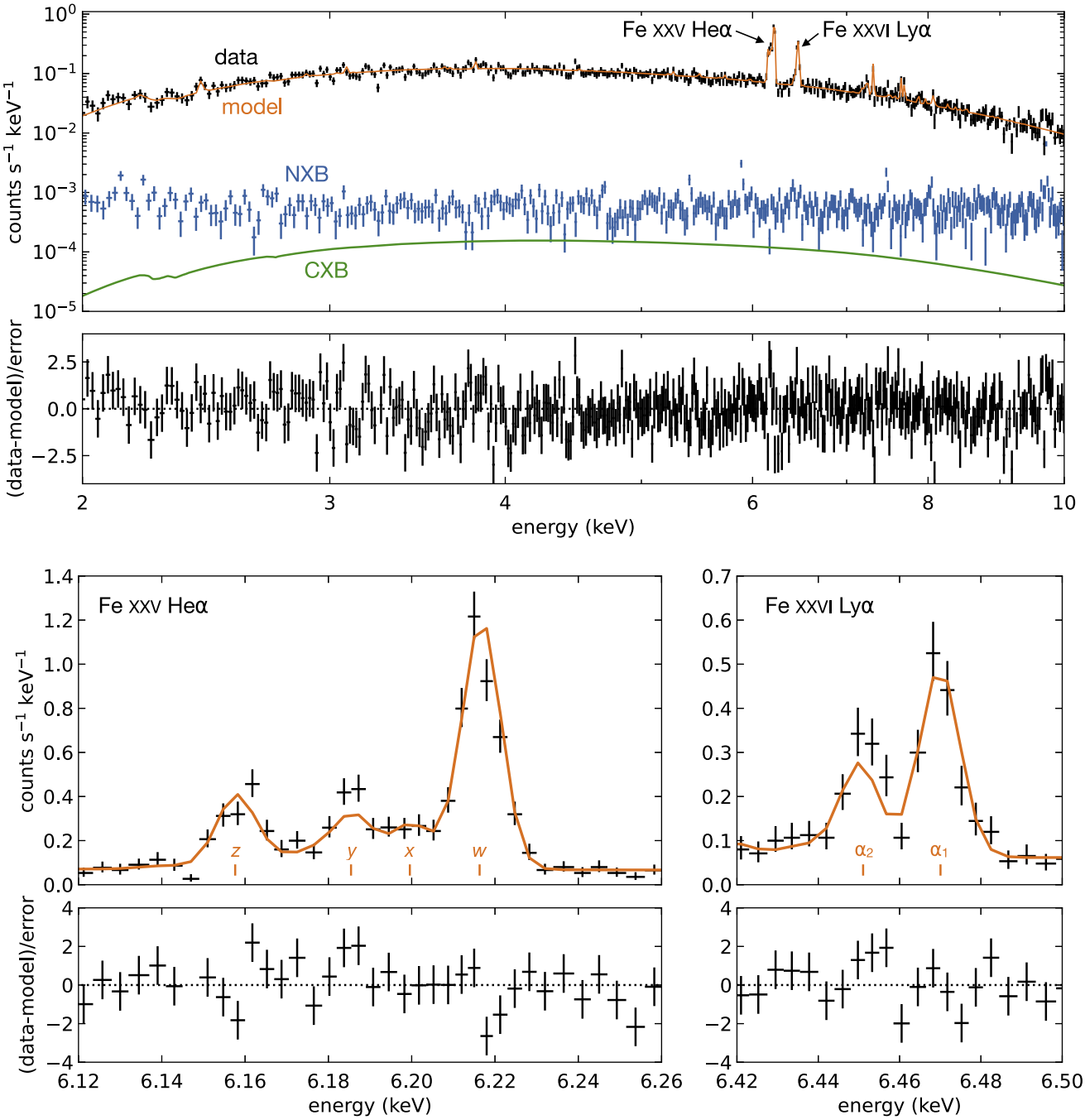

Figure 2. (Top) Broadband Resolve spectrum of the center of A2029, with the two observations summed for clarity. The best-fit 1T `AtomDB` model is shown in orange. The NXB extracted from observations of the dark limb of the Earth is shown in blue and is at least 1 order of magnitude below the cluster emission at all energies. Similarly, the estimated unresolved cosmic X-ray background shown in green is well below the cluster emission. (Bottom) Resolve spectrum zoomed into the strongest emission features of He-like (left) and H-like (right) Fe, as these lines dominate the velocity fit. The individual components of each line complex are distinguishable; in the He-like triplet, these are the forbidden (z), intercombination (y, x), and resonance (w) transitions. The fit residuals show no systematic features around these sharp emission lines, although there are some deviations that are discussed in the text.

identical redshift and velocity broadening within the uncertainty. This indicates that these complexes dominate our leverage on ICM velocity, a fact also apparent from their visual prominence in the spectrum. We estimate the systematic instrumental uncertainty in $v_{\rm bulk}$ to be $\pm 10\,{\rm km\,s^{-1}}$, based on the 0.2 eV gain uncertainty described in Section 2 for energies near 6 keV. The systematic uncertainty in the line-of-sight velocity dispersion is $\pm 3\,{\rm km\,s^{-1}}$, based on propagating the 0.3 eV FWHM uncertainty of the underlying core instrumental line-spread function.

The total background is negligible compared to the observed source spectrum. The NXB spectral flux is at least 1 order of magnitude lower than that of A2029 at all energies across the 2–10 keV band (blue points in Figure 2, left). We estimated the contribution from unresolved background AGN (the cosmic X-ray background; green line in Figure 2, left) using observations from Suzaku (M. W. Bautz et al. 2009), which has a similar PSF to XRISM. This contribution is even lower than the NXB. We have therefore excluded the background from our spectral fits.

Resonant scattering could suppress the flux of the strongest w (resonance) line in the He-like Fe Kα complex. Following the method used for the Hitomi observation of Perseus (Hitomi Collaboration et al. 2018a), we checked that the effect is not detectable in the considered region with the current exposure time by repeating the modeling with and without this line. There was no significant effect on the velocity measurements. We also note that the observed flux of the y intercombination line within the He-like Fe Kα line complex is considerably higher than the model predicts. This does not affect the velocity measurements. We comment on both of these effects in the context of future work in the next section.

3.2. Velocity Structure of the Hot ICM

In Table 1, we estimated the line-of-sight bulk velocity of the gas relative to the BCG as -11^{+12}_{-7} km s^{-1}, averaging over the similar results from the four spectral fits. Taking the quadrature sum of the statistical error, the BCG redshift uncertainty (± 30 km s^{-1}), and the instrumental uncertainty (± 10 km s^{-1}), the 3σ upper limit of bulk velocity becomes $|v| < 100$ km s^{-1}. This indicates no significant line-of-sight velocity difference between the BCG and the ICM. While this result is consistent within the error range of previous Suzaku X-ray Imaging Spectrometer measurements of the central region (N. Ota & H. Yoshida 2016), the upper limit has become an order of magnitude stricter. Therefore, the bulk motion is neglected in the following pressure calculation.

The central galaxy hosts the powerful wide-angle tail radio source PKS 1508+059 (A. D. Lewis et al. 2002; R. Paterno-Mahler et al. 2013; C. G. Martz et al. 2020), extending 40 kpc into the atmosphere (see Figure 1). Despite its high radio power of $P_{1.4} = 10^{41}$ erg s^{-1}, X-ray cavities are absent. Cavities that may have formed earlier in the development of the radio source were possibly destroyed by the sloshing spiral or by hydrodynamical instabilities (R. Paterno-Mahler et al. 2013). Applying the K. W. Cavagnolo et al. (2010) scaling relation between synchrotron power and mechanical power, we find a total mechanical power of $\sim 3 \times 10^{44}$ erg s^{-1}. Assuming the radio source has remained active for 10^7 yr–10^8 yr, it would have deposited 10^{59-60} erg into the atmosphere. The atmospheric gas mass encompassed by the Resolve pointing is $4 \times 10^{12}\, M_\odot$ based on a Chandra X-ray imaging analysis. The total kinetic energy of the atmosphere implied by $\sigma_v \approx 170$ km s^{-1} is then 3.5×10^{60} erg. Therefore, the central radio jet could have contributed a few to several tens of percent of the atmospheric kinetic energy within the pointing. This assumes no other sources of extrathermal motions (e.g., turbulence). A full analysis that includes a subgrid estimate of the velocity dispersion near the jet and a comparison to the off-nuclear pointing will appear in a future paper.

The velocity dispersion of 169 ± 10 km s^{-1} reported here for the central region of A2029 is low in comparison with the sound speed in the system. For a mean temperature of 6.8 keV, the sound speed in the medium is $c_s = (\gamma k_B T/\mu m_p)^{1/2} \approx 1340$ km s^{-1}, with $\gamma = 5/3$ the adiabatic index and $\mu = 0.61$ the mean molecular weight in a fully ionized plasma. If the velocity dispersion determined by Resolve is entirely ascribed to isotropic turbulence, our measurement implies a turbulent Mach number $\mathcal{M}_{3D} = \sqrt{3}\,\sigma_v/c_s \approx 0.22$; turbulent motions are highly subsonic. The resulting NT pressure fraction becomes (D. Eckert et al. 2019)

$$\frac{P_{NT}}{P_{tot}} = \frac{\mathcal{M}^2_{3D}}{\mathcal{M}^2_{3D} + 3/\gamma} = 0.026 \pm 0.003 \quad (1)$$

where we assume that all NT pressure comes from turbulence and ignore contributions from other NT components such as magnetic fields and cosmic rays (F. Miniati & A. Beresnyak 2016; S. Ettori & D. Eckert 2022). The uncertainty in the NT pressure fraction is calculated from the statistical uncertainties in the best-fit velocity dispersion and temperature of the 1T AtomDB model.

In comparison with the core of the Perseus cluster (Hitomi Collaboration et al. 2016, 2018a, 2018b), we measure a similar velocity dispersion in a more massive cluster, such that the limit on the NT pressure fraction is even more stringent. The absence of obvious AGN feedback features in A2029 may explain the lower NT pressure fraction in this cluster compared to Perseus, although the observations probe very different physical scales in the two clusters.

Such a low level of turbulence-induced NT pressure is consistent with estimates based on indirect methods, including gas pressure, density, and temperature power spectra (e.g., P. Schuecker et al. 2004; I. Zhuravleva et al. 2014, 2018; S. Dupourqué et al. 2023, 2024; A. Heinrich et al. 2024; L. Lovisari et al. 2024), universal ICM gas fraction (D. Eckert et al. 2019; S. Ettori & D. Eckert 2022; R. Wicker et al. 2023), and 3D multiprobe reconstructions (K. Umetsu et al. 2015, 2022; J. Sayers et al. 2021). All of these methods imply a low level of NT pressure in cluster cores (<10%), in agreement with direct high-resolution X-ray measurements in Perseus and now A2029. Studies of the NT pressure fraction in cosmological simulations predict that it should increase with radius, from ~10% in cluster cores to ~30% at the virial radius (e.g., E. T. Lau et al. 2009; F. Vazza et al. 2009, 2018; K. Nelson et al. 2014; V. Biffi et al. 2016; M. Angelinelli et al. 2020; G. Gianfagna et al. 2023). However, there exists some level of discrepancy on the impact of NT pressure in cluster cores between studies using different hydrodynamical solvers (adaptive mesh refinement or smoothed particle hydrodynamics) and implementing different baryonic physics (AGN feedback, cooling, and star formation). Additionally, it is unclear whether the calculation of the NT pressure fraction in simulations should be done using the entire velocity field or random gas motions only (F. Vazza et al. 2018; M. Angelinelli et al. 2020).

Recently, N. Truong et al. (2024) studied the level of NT pressure in the cores of Perseus-like clusters in the `TNG-Cluster` simulation set (D. Nelson et al. 2024), which provides resimulations of a sample of >300 massive clusters with the IllustrisTNG model (A. Pillepich et al. 2018). The median NT pressure fraction inferred from mock XRISM data is ~8%, with some systems exhibiting NT pressure fractions as large as ~15%. Our measurement of A2029 occupies the lower end of the N. Truong et al. (2024) distribution in a system that is more massive than Perseus.

We note that A2029 is an exceptionally relaxed-looking cluster away from the core. Even within the core, the sloshing structure is very low in contrast compared to other cluster cool cores, and simulations show that sloshing should last for many Gyr after the disturbing event. In A2029, it appears that event occurred several Gyr ago. The AGN is currently bright in the

radio, but there is no evidence in the X-rays of any AGN-driven mechanical disturbance. These characteristics, combined with the low NT pressure support inferred from the low XRISM velocity dispersion, suggest the cluster may currently be in a quiescent phase of AGN feedback (i.e., no active energy pumping into the ICM at this stage), with any recent minor merger only having enough time to mildly perturb the gas velocity.

Two results from our focused study require future work to fully understand. First, the lack of measurable resonant scattering is at first glance puzzling, given the low velocity dispersion and the detection of resonant scattering in Perseus (Hitomi Collaboration et al. 2018a). Indeed, using the model presented by I. Zhuravleva et al. (2013), we predict that the optical depth at the center of the Fe XXV Heα w component should be higher in A2029 ($\tau \sim 3$) than in Perseus ($\tau \sim 2$). However, we estimate that more than 150 ks is required to significantly detect the change in line strength at the current sensitivity of Resolve. Our 37 ks observation is simply not deep enough compared to the 244 ks Hitomi observation of the Perseus core. A deeper XRISM observation approved for the first General Observer cycle may robustly detect resonant scattering in A2029. Second, several transitions are brighter in Figure 2 than predicted by either the 1T or 2T models, notably the Fe XXV Heα y intercombination line and the Fe XXVI Lyα_2 resonance component. The former is not due to resonant scattering as it persists even when the resonance (w) line is excluded from the fit. It could result from multitemperature structure, and this will be explored in a future paper. The residuals around the Lyα_2 are unexplained at this time. Future work will compare this feature in A2029 to that in other thermal plasmas observed with Resolve to understand if there is a systematic effect.

Our results here from an observation of modest depth demonstrate the power of XRISM to measure line-of-sight velocity structure in galaxy clusters. Additional XRISM measurements in several other systems and out to larger radii in A2029 are currently being analyzed or planned for observation. This larger data set will allow us to compare measurements of the NT pressure fraction over a sizable cluster sample spanning a range of dynamical states and to constrain the importance of NT pressure in the outer regions of clusters where AGN activity should be less important.

Acknowledgments

We gratefully acknowledge the hard work over many years of all of the engineers and scientists who made the XRISM mission possible. Part of this work was performed under the auspices of the US Department of Energy by Lawrence Livermore National Laboratory under Contract DE-AC52-07NA27344. The material is based upon work supported by NASA under award numbers 80GSFC21M0002 and 80GSFC24M0006. This work was supported by JSPS KAKENHI grant numbers JP22H00158, JP22H01268, JP22K03624, JP23H04899, JP21K13963, JP24K00638, JP24K17105, JP21K13958, JP21H01095, JP23K20850, JP24H00253, JP21K03615, JP24K00677, JP20K14491, JP23H00151, JP19K21884, JP20H01947, JP20KK0071, JP23K20239, JP24K00672, JP24K17104, JP24K17093, JP20K04009, JP21H04493, JP20H01946, JP23K13154, JP19K14762, JP20H05857, JP23H00121, JP23K22540, JP25287042, and JP23K03459. This work was supported by NASA grant numbers 80NSSC20K0733, 80NSSC18K0978, 80NSSC20K0883, 80NSSC20K0737, 80NSSC24K0678, 80NSSC18K1684, 80NSSC23K0650, and 80NNSC22K1922. L.C. acknowledges support from NSF award 2205918. C.D. acknowledges support from STFC through grant ST/T000244/1. L.G. acknowledges financial support from Canadian Space Agency grant 18XARMSTMA. M.S. acknowledges the support by the RIKEN Pioneering Project Evolution of Matter in the Universe (r-EMU) and Rikkyo University Special Fund for Research (Rikkyo SFR). A.T. and the present research are in part supported by the Kagoshima University postdoctoral research program (KU-DREAM). S.Y. acknowledges support by the RIKEN SPDR Program. I.Z. acknowledges partial support from the Alfred P. Sloan Foundation through the Sloan Research Fellowship. SE acknowledges the financial contribution from the contracts Prin-MUR 2022 supported by Next Generation EU (M4.C2.1.1, n.20227RNLY3 The concordance cosmological model: stress tests with galaxy clusters), ASI-INAF Athena 2019-27-HH.0, "Attività di Studio per la comunità scientifica di Astrofisica delle Alte Energie e Fisica Astroparticellare" (Accordo Attuativo ASI-INAF n. 2017-14-H.0), and from the European Union's Horizon 2020 Programme under the AHEAD2020 project (grant agreement No. 871158). This work was supported by the JSPS Core-to-Core Program, JPJSCCA20220002. The material is based on work supported by the Strategic Research Center of Saitama University.

ORCID iDs

Marc Audard https://orcid.org/0000-0003-4721-034X
Ralf Ballhausen https://orcid.org/0000-0002-1118-8470
Aya Bamba https://orcid.org/0000-0003-0890-4920
Ehud Behar https://orcid.org/0000-0001-9735-4873
Rozenn Boissay-Malaquin https://orcid.org/0000-0003-2704-599X
Laura Brenneman https://orcid.org/0000-0003-2663-1954
Gregory V. Brown https://orcid.org/0000-0001-6338-9445
Lia Corrales https://orcid.org/0000-0002-5466-3817
Elisa Costantini https://orcid.org/0000-0001-8470-749X
Renata Cumbee https://orcid.org/0000-0001-9894-295X
Maria Diaz Trigo https://orcid.org/0000-0001-7796-4279
Chris Done https://orcid.org/0000-0002-1065-7239
Ken Ebisawa https://orcid.org/0000-0002-5352-7178
Megan E. Eckart https://orcid.org/0000-0003-3894-5889
Dominique Eckert https://orcid.org/0000-0001-7917-3892
Satoshi Eguchi https://orcid.org/0000-0003-2814-9336
Teruaki Enoto https://orcid.org/0000-0003-1244-3100
Adam Foster https://orcid.org/0000-0003-3462-8886
Ryuichi Fujimoto https://orcid.org/0000-0002-2374-7073
Yutaka Fujita https://orcid.org/0000-0003-0058-9719
Yasushi Fukazawa https://orcid.org/0000-0002-0921-8837
Kotaro Fukushima https://orcid.org/0000-0001-8055-7113
Luigi Gallo https://orcid.org/0009-0006-4968-7108
Javier A. García https://orcid.org/0000-0003-3828-2448
Liyi Gu https://orcid.org/0000-0001-9911-7038
Matteo Guainazzi https://orcid.org/0000-0002-1094-3147
Kouichi Hagino https://orcid.org/0000-0003-4235-5304
Kenji Hamaguchi https://orcid.org/0000-0001-7515-2779
Isamu Hatsukade https://orcid.org/0000-0003-3518-3049
Katsuhiro Hayashi https://orcid.org/0000-0001-6922-6583
Takayuki Hayashi https://orcid.org/0000-0001-6665-2499
Natalie Hell https://orcid.org/0000-0003-3057-1536

Edmund Hodges-Kluck https://orcid.org/0000-0002-2397-206X
Ann Hornschemeier https://orcid.org/0000-0001-8667-2681
Yuto Ichinohe https://orcid.org/0000-0002-6102-1441
Jelle Kaastra https://orcid.org/0000-0001-5540-2822
Timothy Kallman https://orcid.org/0000-0002-5779-6906
Erin Kara https://orcid.org/0000-0003-0172-0854
Satoru Katsuda https://orcid.org/0000-0002-1104-7205
Yoshiaki Kanemaru https://orcid.org/0000-0002-4541-1044
Richard Kelley https://orcid.org/0009-0007-2283-3336
Caroline Kilbourne https://orcid.org/0000-0001-9464-4103
Shunji Kitamoto https://orcid.org/0000-0001-8948-7983
Shogo Kobayashi https://orcid.org/0000-0001-7773-9266
Takayoshi Kohmura https://orcid.org/0000-0003-4403-4512
Maurice Leutenegger https://orcid.org/0000-0002-3331-7595
Michael Loewenstein https://orcid.org/0000-0002-1661-4029
Yoshitomo Maeda https://orcid.org/0000-0002-9099-5755
Maxim Markevitch https://orcid.org/0000-0003-0144-405
Kyoko Matsushita https://orcid.org/0000-0003-2907-0902
Dan McCammon https://orcid.org/0000-0001-5170-4567
Brian McNamara https://orcid.org/0000-0002-2622-2627
François Mernier https://orcid.org/0000-0002-7031-4772
Eric D. Miller https://orcid.org/0000-0002-3031-2326
Jon M. Miller https://orcid.org/0000-0003-2869-7682
Ikuyuki Mitsuishi https://orcid.org/0000-0002-9901-233X
Misaki Mizumoto https://orcid.org/0000-0003-2161-0361
Tsunefumi Mizuno https://orcid.org/0000-0001-7263-0296
Koji Mori https://orcid.org/0000-0002-0018-0369
Koji Mukai https://orcid.org/0000-0002-8286-8094
Richard Mushotzky https://orcid.org/0000-0002-7962-5446
Hiroshi Nakajima https://orcid.org/0000-0001-6988-3938
Kazuhiro Nakazawa https://orcid.org/0000-0003-2930-350X
Jan-Uwe Ness https://orcid.org/0000-0003-0440-7193
Kumiko Nobukawa https://orcid.org/0000-0002-0726-7862
Masayoshi Nobukawa https://orcid.org/0000-0003-1130-5363
Hirofumi Noda https://orcid.org/0000-0001-6020-517X
Shoji Ogawa https://orcid.org/0000-0002-5701-0811
Anna Ogorzalek https://orcid.org/0000-0003-4504-2557
Takashi Okajima https://orcid.org/0000-0002-6054-3432
Naomi Ota https://orcid.org/0000-0002-2784-3652
Stephane Paltani https://orcid.org/0000-0002-8108-9179
Robert Petre https://orcid.org/0000-0003-3850-2041
Paul Plucinsky https://orcid.org/0000-0003-1415-5823
Frederick S. Porter https://orcid.org/0000-0002-6374-1119
Katja Pottschmidt https://orcid.org/0000-0002-4656-6881
Makoto Sawada https://orcid.org/0000-0003-2008-6887
Megumi Shidatsu https://orcid.org/0000-0001-8195-6546
Aurora Simionescu https://orcid.org/0000-0002-9714-3862
Randall Smith https://orcid.org/0000-0003-4284-4167
Hiromasa Suzuki https://orcid.org/0000-0002-8152-6172
Andrew Szymkowiak https://orcid.org/0000-0002-4974-687X
Hiromitsu Takahashi https://orcid.org/0000-0001-6314-5897
Toru Tamagawa https://orcid.org/0000-0002-8801-6263
Takaaki Tanaka https://orcid.org/0000-0002-4383-0368
Atsushi Tanimoto https://orcid.org/0000-0002-0114-5581
Makoto Tashiro https://orcid.org/0000-0002-5097-1257
Yukikatsu Terada https://orcid.org/0000-0002-2359-1857
Yuichi Terashima https://orcid.org/0000-0003-1780-5481
Yohko Tsuboi https://orcid.org/0000-0001-9943-0024
Masahiro Tsujimoto https://orcid.org/0000-0002-9184-5556
Takeshi Tsuru https://orcid.org/0000-0002-5504-4903
Hiroyuki Uchida https://orcid.org/0000-0003-1518-2188
Nagomi Uchida https://orcid.org/0000-0002-5641-745X
Yuusuke Uchida https://orcid.org/0000-0002-7962-4136
Hideki Uchiyama https://orcid.org/0000-0003-4580-4021
Yoshihiro Ueda https://orcid.org/0000-0001-7821-6715
Jacco Vink https://orcid.org/0000-0002-4708-4219
Shin Watanabe https://orcid.org/0000-0003-0441-7404
Brian J. Williams https://orcid.org/0000-0003-2063-381X
Satoshi Yamada https://orcid.org/0000-0002-9754-3081
Shinya Yamada https://orcid.org/0000-0003-4808-893X
Hiroya Yamaguchi https://orcid.org/0000-0002-5092-6085
Kazutaka Yamaoka https://orcid.org/0000-0003-3841-0980
Noriko Yamasaki https://orcid.org/0000-0003-4885-5537
Makoto Yamauchi https://orcid.org/0000-0003-1100-1423
Mihoko Yukita https://orcid.org/0000-0001-6366-3459
Irina Zhuravleva https://orcid.org/0000-0001-7630-8085
Tommaso Bartalesi https://orcid.org/0009-0004-5838-2213
Stefano Ettori https://orcid.org/0000-0003-4117-8617
Lorenzo Lovisari https://orcid.org/0000-0002-3754-2415
Tom Rose https://orcid.org/0000-0002-8310-2218
Arnab Sarkar https://orcid.org/0000-0002-5222-1337
Ming Sun https://orcid.org/0000-0001-5880-0703
Prathamesh Tamhane https://orcid.org/0000-0001-8176-7665

References

Andrade-Santos, F., Jones, C., Forman, W. R., et al. 2017, ApJ, 843, 76
Angelinelli, M., Vazza, F., Giocoli, C., et al. 2020, MNRAS, 495, 864
Arnaud, K. A. 1996, in ASP Conf. Ser. 101, Astronomical Data Analysis Software and Systems V, ed. G. H. Jacoby & J. Barnes (San Francisco, CA: ASP), 17
Bautz, M. W., Miller, E. D., Sanders, J. S., et al. 2009, PASJ, 61, 1117
Biffi, V., Borgani, S., Murante, G., et al. 2016, ApJ, 827, 112
Cash, W. 1979, ApJ, 228, 939
Cassano, R., Ettori, S., Giacintucci, S., et al. 2010, ApJL, 721, L82
Cavagnolo, K. W., McNamara, B. R., Nulsen, P. E. J., et al. 2010, ApJ, 720, 1066
Clarke, T. E., Blanton, E. L., & Sarazin, C. L. 2004, ApJ, 616, 178
Dullo, B. T., Graham, A. W., & Knapen, J. H. 2017, MNRAS, 471, 2321
Dupourqué, S., Clerc, N., Pointecouteau, E., et al. 2023, A&A, 673, A91
Dupourqué, S., Clerc, N., Pointecouteau, E., et al. 2024, A&A, 687, A58
Eckart, M. E., Brown, G. V., Chiao, M. P., et al. 2024, Proc. SPIE, 13093, 130931P
Eckert, D., Ettori, S., Robertson, A., et al. 2022, A&A, 666, A41
Eckert, D., Ghirardini, V., Ettori, S., et al. 2019, A&A, 621, A40
Eckert, D., Jauzac, M., Shan, H., et al. 2015, Natur, 528, 105
Ettori, S., & Eckert, D. 2022, A&A, 657, L1
Foster, A. R., Ji, L., Smith, R. K., & Brickhouse, N. S. 2012, ApJ, 756, 128
Gatuzz, E., Sanders, J. S., Dennerl, K., et al. 2022a, MNRAS, 511, 4511
Gatuzz, E., Sanders, J. S., Canning, R., et al. 2022b, MNRAS, 513, 1932
Gatuzz, E., Sanders, J. S., Dennerl, K., et al. 2023, MNRAS, 522, 2325
Gianfagna, G., Rasia, E., Cui, W., et al. 2023, MNRAS, 518, 4238
Heinrich, A., Zhuravleva, I., Zhang, C., et al. 2024, MNRAS, 528, 7274
HI4PI Collaboration, Ben Bekhti, N., Flöer, L., et al. 2016, A&A, 594, A116
Hitomi Collaboration, Aharonian, F., Akamatsu, H., et al. 2016, Natur, 535, 117
Hitomi Collaboration, Aharonian, F., Akamatsu, H., et al. 2018a, PASJ, 70, 10
Hitomi Collaboration, Aharonian, F., Akamatsu, H., et al. 2018b, PASJ, 70, 9
Ishisaki, Y., Kelley, R. L., & Awaki, H. 2022, Proc. SPIE, 12181, 121811S

Kaastra, J. S., & Bleeker, J. A. M. 2016, A&A, 587, A151
Kaastra, J. S., Mewe, R., & Nieuwenhuijzen, H. 1996, in 11th Colloquium on UV and X-ray Spectroscopy of Astrophysical and Laboratory Plasmas, SPEX: a new code for spectral analysis of X & UV spectra, ed. K. Yamashita & T. Watanabe, 411
Kravtsov, A. V., & Borgani, S. 2012, ARA&A, 50, 353
Lau, E. T., Kravtsov, A. V., & Nagai, D. 2009, ApJ, 705, 1129
Lewis, A. D., Stocke, J. T., & Buote, D. A. 2002, ApJL, 573, L13
Lodders, K., & Palme, H. 2009, M&PSA, 72, 5154
Lovisari, L., Ettori, S., Rasia, E., et al. 2024, A&A, 682, A45
Markevitch, M., & Vikhlinin, A. 2007, PhR, 443, 1
Martz, C. G., McNamara, B. R., Nulsen, P. E. J., et al. 2020, ApJ, 897, 57
Miniati, F., & Beresnyak, A. 2016, IAUFM, 29B, 700
Nelson, D., Pillepich, A., Ayromlou, M., et al. 2024, A&A, 686, A157
Nelson, K., Lau, E. T., & Nagai, D. 2014, ApJ, 792, 25
Ota, N., & Yoshida, H. 2016, PASJ, 68, S19
Paterno-Mahler, R., Blanton, E. L., Randall, S. W., & Clarke, T. E. 2013, ApJ, 773, 114
Pillepich, A., Springel, V., Nelson, D., et al. 2018, MNRAS, 473, 4077
Porter, F. S., Kilbourne, C. A., Chiao, M., et al. 2024, Proc. SPIE, 13093, 130931K
Prasad, D., Voit, G. M., & O'Shea, B. W. 2024, MNRAS, 531, 259
Reiprich, T. H., Veronica, A., Pacaud, F., et al. 2021, A&A, 647, A2
Rossetti, M., Gastaldello, F., Eckert, D., et al. 2017, MNRAS, 468, 1917
Sanders, J. S., Dennerl, K., Russell, H. R., et al. 2020, A&A, 633, A42
Sarkar, A., Randall, S., Su, Y., et al. 2022, ApJL, 935, L23
Sarkar, A., Randall, S., Su, Y., et al. 2023, ApJ, 944, 132
Sayers, J., Sereno, M., Ettori, S., et al. 2021, MNRAS, 505, 4338
Schuecker, P., Finoguenov, A., Miniati, F., Böhringer, H., & Briel, U. G. 2004, A&A, 426, 387
Simionescu, A., ZuHone, J., Zhuravleva, I., et al. 2019, SSRv, 215, 24
Sohn, J., Geller, M. J., Walker, S. A., et al. 2019, ApJ, 871, 129
Tamura, T., Hayashida, K., Ueda, S., & Nagai, M. 2011, PASJ, 63, S1009
Tashiro, M., Maejima, H., & Toda, K. 2020, Proc. SPIE, 11444, 1144422
Truong, N., Pillepich, A., Nelson, D., et al. 2024, A&A, 686, A200
Umetsu, K., Sereno, M., Medezinski, E., et al. 2015, ApJ, 806, 207
Umetsu, K., Ueda, S., Hsieh, B.-C., et al. 2022, ApJ, 934, 169
Vazza, F., Angelinelli, M., Jones, T. W., et al. 2018, MNRAS, 481, L120
Vazza, F., Brunetti, G., Kritsuk, A., et al. 2009, A&A, 504, 33
Werner, N., Finoguenov, A., Kaastra, J. S., et al. 2008, A&A, 482, L29
Wicker, R., Douspis, M., Salvati, L., & Aghanim, N. 2023, A&A, 674, A48
Wilms, J., Allen, A., & McCray, R. 2000, ApJ, 542, 914
XRISM Collaboration 2024, PASJ, 76, 1186
Zhuravleva, I., Allen, S. W., Mantz, A., & Werner, N. 2018, ApJ, 865, 53
Zhuravleva, I., Churazov, E., Schekochihin, A. A., et al. 2014, Natur, 515, 85
Zhuravleva, I., Churazov, E., Sunyaev, R., et al. 2013, MNRAS, 435, 3111
ZuHone, J. A., Markevitch, M., & Johnson, R. E. 2010, ApJ, 717, 908
ZuHone, J. A., Miller, E. D., Bulbul, E., & Zhuravleva, I. 2018, ApJ, 853, 180